A distributed stochastic perception-action loop model of cell motility

Moritz Buck[*†§], Deniz Saltukoglu[*], Melanie Boerries[*†], Matias Simons[*‡] and Hauke Busch[*†§]

[*]*Centre for Systems Biology (ZBSA)*
University of Freiburg
Freiburg, Germany

[†]*FRIAS, LifeNet*
University of Freiburg
Freiburg, Germany

[‡]*Renal division*
University Hospital of Freiburg
Freiburg, Germany

[§]*Corresponding authors: moritz.buck@zbsa.uni-freiburg.de, hauke.busch@frias.uni-freiburg.de*

Abstract

In this paper, we present a novel framework for the modeling of cell-migration, and more specifically the migration of human keratinocytes. The model decouples the embodiment of an artificial cell into two elements. A cell-body is implemented by two sets of springs forming a membrane and a supporting cortical-cytoskeleton, which allows for cell-body rigidity and flexibility. The leading-edge, a structure spreading around the cell-body, is simulated with a stochastic cellular-automata. It defines the migratory forces that pull the cell-body according to its local spread around the cell. The overall movement of the leading-edge depends on stochastic interaction with the environment and guides the whole cell movement through spatio-temporal integration of local forces. We demonstrate that our cell migration model allows for spontaneous symmetry-breaking and directed cell movement and has in-built obstacle-avoidance, closely mimicking the migration of living cells. The model is extended to simulate chemotactic behavior, the artificial cell can sense and move along a gradient with its trajectory depending on the cell shape, stiffness and leading-edge dynamics. In summary, we have developed a novel cell migration model with emergent properties, wherein local forces create an integrated cell movement. The presented interplay of the distributed physical and an informational embodiment is not limited in reach to the example of cell migration, but can of interest for design of perception-action loops and sensor evolution in general.

1. Introduction

In the context of robotics and artificial life, perception-action loops are generally viewed as an arbitrarily complex mapping from sensory input to a motor output [1], [2]. The sensory input is a representation of the environment, which, through filters and classifiers of any possible form, is processed into a motor action. Living cells also respond to environmental cues through perception and action. They can sense light, chemical or electrical signals, or other cells, and react accordingly. Most of the sensing resides at the membrane, where protein-complexes respond to the signal and then either trigger an internal signaling cascade and/or some local reaction. Eventually, this causes changes in motion of the whole cell through re-organization of changed dynamics of the cytoskeleton or individual cellular motors. These perception-action loops can be highly distributed and multi-layered, as the whole membrane of a cell can act as a highly distributed sensor, and often as an agent of motion as well.

The study of cell motility and cell migration is a long standing topic. Various modes of cell movement are known so far [3]: movement through rotating or beating flagella in bacteria [4] or spermatozoa [5], respectively; Crawling or gliding has been investigated in slime-molds [6] and single-celled protozoa [7], [8]. Parallel to the many modes of cell movement in various organisms, a plethora of mathematical models has been developed to describe them. ODE- and PDE-based models have been developed to simulate molecular motors [9], [10] or cilia motion[11]. There are cellular automata-based models of neural stem cell migration [12], cellular Potts models [13] or complex finite-element methods [14] to study chemotaxis. The Cell Migration Consortium (http://www.cellmigration.org/) contains a large collection of models, that give a good overview on the current biological knowledge and mathematical modeling approaches.

Here, we present a cellular-automata based model

of keratinocyte cell migration in two dimensions that captures the physical properties of movement along a gradient of physicochemical cues and obstacle avoidance. Keratinocytes are the cells that make up 95% of the epidermis, the top layer of the human skin. When the skin is injured these cells start migrating to close the wound. Three types of signals are known to direct keratinocytes during wound healing: chemical signals mediated by soluble molecules [15], receptor activation on the cell surface through direct cell contact [16], [17], and electrical field gradients [18]. The goal of our modeling approach is to understand how the above environmental signals are translated into a directed cell movement. The experimental data is based on individually plated keratinocytes moving in two dimensions on a coated surface (Fig. 1). Isolated keratinocytes randomly polarize and start "crawling". When moving, the cells develop a protruding leading-edge, the lamellipodium, that moves ahead of the rather rigid cell-body. The lamellipodium is a thin, highly dynamic structure. It contains an interwoven mesh of actin fibers, which are part of the cytoskeleton, that pushes and pulls the cell membrane and thereby determining the cell morphology. If a chemical or electric cue is applied, the keratinocyte changes direction along the gradient of the stimulus by turning and reorganizing its lamellipodium. How the keratinocytes senses the chemical or electrical gradient and turn accordingly is still unclear.

Most modeling approaches for cell migration focus on the mechanical characteristics of the actin dynamics that determine the cell movement [19]. However, there is still a lack of experimental data due to the difficulty to quantify the actin and membrane dynamics. Here, we develop a model for keratinocyte movement within an *in silico* environment that links external stimuli to whole cell movements, while retaining the possibility of complex dynamics. From this model we then want to extract ideas about how an external cue is transformed into the observed motion of keratinocytes, e.g. the perception-action loop that guides it.

Our artificial cell model needs to be rotationally invariant and must show spontaneous symmetry breaking properties. Moreover, the cell-body and the leading-edge ought to have a flexible cell morphology to mimic the spatial adaptation of a keratinocyte to external physical forces like pressure or stress. The sensory inputs are integrated locally along the cell membrane to allow for a differential sensing of chemical gradients on the cell surface [21]. For model optimization and fitting to experimental data, the model needs to have as few parameters as possible. Its output should ideally correspond to biologically quantifiable variables and
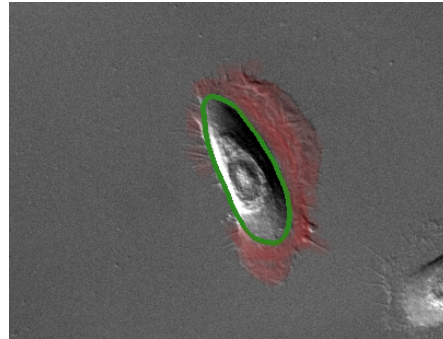

Figure 1. An human keratinocyte migrating on a coated surface. The cell-body is outlined in green, the flattened lamellipodium forming the leading-edge is highlighted in red. The keratinocyte is moving from left to right. Also see Video 1 on [20].

readouts. Previously developed cell migration models that are based on frameworks such as the cellular Potts model [22], Braitenberg vehicles [23], or agent-based systems [24] do not conform to all criteria above.

The model reduces the migrating keratinocyte to two main components: the cell-body and the leading-edge. The former is implemented by a connected-spring model moving on a discrete spatial grid under the influence of noise (Section 2.2). This cell-body "senses" the environment through a highly dynamical "leading-edge", whose size and location is updated in a cellular-automata-like fashion [25]. It spreads on a 2D grid according to a set of stochastic update rules that depend on the environment (Section 2.3).

Taken together, we present a novel model for cell migration that is able to show symmetry breaking, sense the environment and can follow chemical gradients.

2. Model

2.1. Environment

The cell-body and the leading-edge are embedded in a well defined environment, the space in which the cell can move. It is defined on a discrete grid $\mathcal{G}$

$$\mathcal{G} = \{ \text{ all } (x,y) \in \mathbb{Z}^{+2}, \text{ where } x \leq x_{\max}, y \leq y_{\max} \},$$

which defines the positions of all elements of the artificial cell and the environment.

For all of the experiments presented here, the 2D-grid is bounded with Dirichlet boundary conditions. We use a discrete and uniform pseudo-synchronous update of the system, where all elements of the system are updated once each time-step, but in a random order.
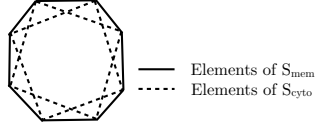
2.2. The cell-body

Figure 2. A cell-body with $n = 8$. The solid lines denote the springs constituting the membrane, the dashed lines the cortical cytoskeleton.

The cell-body is simulated as a deformable connected-spring model that allows the cell to change its shape and to respond to external forces and shear stresses. This mimics the opposing forces in real cells that determine the cell morphology: the contractile force of the lipid membrane of the cell and the actin cytoskeleton, that supports and changes the cell specific morphology by pushing against the cell membrane. If no forces are applied the cell-body relaxes to a circular shape, and will elongate if the leading-edge exerts a pulling force while moving along the surface. Three assumptions are defining our spring-model: (i) no damping, (ii) high "viscosity" (the displacement is directly proportional to the force applied, no inertia) and (iii) a Gaussian noise term added to the force vector to include a random component in the movement of the cell-body (similar to [26]).

We define a spring ρ by two points in space and two parameters:

$$\rho = \begin{cases} (p_{\text{left}}, p_{\text{right}}) & \in \quad \mathcal{G}^2 \\ (k, l) & \in \quad \mathbb{R}^{+2} \end{cases},$$

with p_{left} and p_{right} being the grid positions of the left and right ends of the spring and k and l denoting the elasticity and the equilibrium length, respectively.

The cell-body itself is defined by n nodes $\mathcal{N}$ that are connected in total by $2n$ springs. Based on their function, the springs are divided into two sets. The first set of springs, S_{mem}, defines the cell-body's membrane, the border between the inside and outside of the cell-body. S_{mem} is composed of n circularly connected springs of equal elasticity k_{mem}, and equilibrium length l_{mem}. To consolidate the shape of the cell-body without introducing additional forces (e.g. torsional forces) or further constraints (e.g. limit angles between springs), an additional set of springs has been added to emulate the cortical-cytoskeleton. This set of springs, S_{cyto}, is also composed with n springs of equal elasticity k_{cyto}, and of equilibrium length $l_{\text{cyto}} = 2\, l_{\text{mem}}$. The springs of S_{cyto} connect the far ends of all the connected pairs of springs of S_{mem}. For

rotational symmetry, each node $\eta_i \in \mathcal{N}$ is connected to four springs with two from S_{mem} and two from S_{cyto} (Fig. 2).
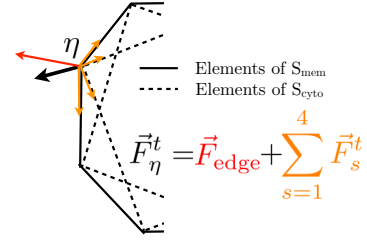

Figure 3. Sum of forces for at the node η. The solid lines denote the springs constituting the membrane, the dashed ones the cortical cytoskeleton. The force in orange are the forces generated by the springs and the one in red represents the force generated by the leading-edge. The black vector is the resulting force.

At each time step t of a simulation a force balance is computed for each node $\eta \in \mathcal{N}$ (dropping the index i of η for simplicity)

$$\vec{F}_\eta(t) = \vec{F}_\eta^{\text{edge}}(t) + \sum_{s=1}^{4} \vec{F}_\eta^s(t),$$

where $\vec{F}_\eta^{\text{edge}}(t)$ is the force generated at time t by the leading-edge at the respective node η (see section 2.3). $\vec{F}_\eta^s(t)$ denotes the force generated at time t by one of the four springs ρ^s attached to the node η under consideration. These forces are calculated with

$$\vec{F}_\eta^s(t) = k_s(l_\eta^s - l^s)\vec{u}_\eta^s(t),$$

where k^s and l^s are k_{mem} and l_{mem}, if $\rho^s \in S_{\text{mem}}$ or k_{cyto} and l_{cyto}, if $\rho^s \in S_{\text{cyto}}$, and $\vec{u}_\eta^s(t)$ is a unitary vector pointing in the negative direction along ρ_η^s. l_η^s denotes the length of ρ_η^s at time t. Note that, if there is no force of the leading-edge exerted on the cell-body (all $\vec{F}_\eta^{\text{edge}}(t) = 0$) the sum of all $\vec{F}_\eta^s(t)$ will be zero, as the forces at opposite ends of all springs cancel out.

As we consider high viscosity, the expected discrete displacement, $\vec{\delta}_\eta(t)$ of η, is proportional to the force

$$\vec{\delta}_\eta(t) \propto \vec{F}_\eta(t).$$

This determines the new expected position $\pi_\eta(t+1)$ of η, after the update

$$\pi_\eta(t+1) = p_\eta(t) + \vec{\delta}_\eta(t),$$

with $p_\eta(t) \in \mathcal{G}$, and $\pi_\eta(t+1) \in \mathbb{R}^2$. To account for noise and discretization we define a neighborhood ω_{p_η} for every element p_η of $\mathcal{G}$ as

$$\omega_{p_\eta} = \{\text{all } q \in \mathcal{G} | d > \|p_\eta - q\|\},$$

where d is a neighborhood radius and $\| * \|$ defines the Euclidean distance. This neighborhood defines all allowed "moves" of the node η from its current position p_η. To determine the true position of η at $t + 1$, we compute a probability distribution over the neighborhood of $p_\eta(t)$ depending on the expected position $\pi_\eta(t+1)$, and then randomly choose one new position $p_\eta(t+1)$ in this neighborhood. The probability of each possible true position is defined as

$$P_q = \frac{1}{P_N} \exp\left[-\frac{\|q - \pi_\eta(t+1)\|^2}{2} \right], \forall q \in \omega_{p_\eta},$$

where P_N is normalizing the probability distribution such that

$$\sum_{\forall q \in \omega_{p_\eta}} P_q = 1.$$

This distribution is then used to pick one element of $\omega_{p_\eta}(t)$ as the next true position $p_\eta(t+1)$ of the node η.

2.3. The leading-edge

The leading-edge of migrating, living cells spreads in their front and pulls the cell forward. It acts under the influence of the cell-body and the environment and has a permanent structural turnover, at times randomly retracting or ruffling. Hence, the leading-edge denotes a dynamic structure that defines what the cell senses and that translates this perception into a set of forces acting on the periphery of the cell-body.

Here, we model the leading-edge as a subset $\mathcal{L}(t)$ of $\mathcal{G}$ that is attached to the cell-body. The shape and size of the leading-edge depends on the cell-body itself and the environment, and changes dynamically. To define $\mathcal{L}(t)$ at time t three subsets of $\mathcal{G}$ are needed. The subsets comprise the grid elements of the inside and outside of the cell-body, denoted as $\mathcal{I}(t)$ and $\mathcal{O}(t)$, as well as the grid points on the border (membrane) between inside and outside, $\mathcal{B}(t)$. A points-in-polygon algorithm generates this partition of $\mathcal{G}$ by checking if the points of the grid lie inside or outside of the polygon defined by S_{mem}. If one of the springs is "crossing" a grid point, it is considered in $\mathcal{B}$.

The dynamics of the leading-edge are defined by the "spreading" and the "detachment" rules. "Spreading" means that at each time-step t, every element in the neighborhood of an element $e \in \mathcal{L}(t)$ has a finite probability of being added to or remaining in $\mathcal{L}$ at time $t + 1$. "Detachment" allows for each element $e \in \mathcal{L}$ to

be removed from the leading-edge at a subsequent time step $t + 1$ with a certain probability. The leading-edge is initialized at $t = 0$ as $\mathcal{L}(t = 0) = \mathcal{B}(t = 0)$. At every time step $t > 0$, Alg. 1 is applied, wherein the functions p_{spread} and p_{detach} denote the probability for each grid point j within the neighborhood of $\mathcal{L}(t)$ to be added or detached from the leading-edge

$$p_{\text{spread}}[j, \mathcal{L}(t)] = p_{\text{spread}}^{\text{basal}} \left[1 - \frac{2\|j - \text{center}[\mathcal{L}(t)]\|}{w_{\text{max}}} \right]$$

and

$$p_{\text{detach}}[j, \mathcal{L}(t)] = p_{\text{detach}}^{\text{basal}} \frac{2\|j - \text{center}[\mathcal{L}(t)]\|}{w_{\text{max}}},$$

where $p_{\text{detach}}^{\text{basal}}$ and $p_{\text{spread}}^{\text{basal}}$ in $[0, 1]$ denote the spreading, and detachment parameters respectively. w_{max} is a shape parameter that controls the average width of the leading-edge. 'center' refers to the location of the center of mass of the leading-edge. Effectively, the probability of spreading is proportional to the basal probability $p_{\text{spread}}^{\text{basal}}$ and decreases with increasing distance from the center of mass of the leading-edge. $p_{\text{spread}}[j, \mathcal{L}(t)]$ becomes 0 at a distance of $w_{\text{max}}/2$ from the center of mass. Conversely, the probability of detaching increases, when moving away from the center of mass.

Without other environmental influences, the leading-edge is a circular structure with decreasing density away from its center, being empty "under" the cell-body. Note, how the latter condition induces symmetry-breaking. At $t = 0$, the centers of the cell-body and the leading-edge coincide. Due to initial random spreading of the leading-edge, a preferential growth direction of $\mathcal{L}$ will be induced from the centre of mass of the leading-edge.

The leading-edge acts on each node η of the cell-body positioned at p_η through the force $\vec{F}_{\text{edge}}$

$$\vec{F}_\eta^{\text{edge}} = \frac{1}{|\mathcal{G}_\eta|} \sum_{e \in \mathcal{L}_\eta} \overrightarrow{e - p_\eta},$$

where $\mathcal{L}_\eta$ are elements of $\mathcal{L}$ within the radius v of p_η, and $|\mathcal{G}_\eta|$ denote the total number of grid points within the radius v of p_η. Through this normalization the force $\vec{F}_\eta^{\text{edge}}$ lies between $[0, 1]$ and scales proportional to the number of grid points belonging to the leading edge within the local neighborhood of η. The vector sum ensures that the force $\vec{F}_\eta^{\text{edge}}$ is directed locally towards highest density of $\mathcal{L}_\eta$. Summing over all nodes of the cell-body, this will induce a coordinated, global pulling behavior of the leading-edge on the cell-body.

Data: $\mathcal{L}_t$, $\mathcal{B}_{t+1}$, $\mathcal{I}_{t+1}$
Result: $\mathcal{L}_{t+1}$
initialize $\mathcal{L}_{t+1}$ with $\mathcal{L}_t$;
add $\mathcal{B}_{t+1}$ to $\mathcal{L}_{t+1}$;
`#spreading rule`
foreach $e \in \mathcal{L}_{t+1}$ **do**
  get neighborhood n;
  foreach $j \in n$ **do**
    get a random number $r \in [0,1]$;
    if $r < p_{spread}(j, \mathcal{L}_t)$ **then**
      add j to $\mathcal{L}_{t+1}$;
    end
  end
end
`#detachment rule`
foreach $j \in \mathcal{L}_{t+1}$ **do**
  get a random number $r \in [0,1]$;
  if $r < p_{detach}(j, \mathcal{L}_t)$ **then**
    remove j from $\mathcal{L}_{t+1}$;
  end
end
remove $\mathcal{I}_{t+1}$ from $\mathcal{L}_{t+1}$;

Algorithm 1: Rule-set describing the spreading of the leading-edge. p_{spread} and p_{detach} are two functions returning a probability depending on the position of j and the shape of the leading-edge at the preceding time step.

3. Experiments

In the following, we will demonstrate the intrinsic capabilities of the cell migration model by three *in silico* experiments, also showing how to implement complex cell behavior. We will first show spontaneous symmetry-breaking and obstacle avoidance by the cell movement. Also we will modify the p_{spread} function to demonstrate its influence on gradient-climbing capabilities.

3.1. Parameters and implementation

For these experiments we have empirically chosen a set of parameters that result in stable cell movement. An rough empirical analysis confirms model stability over a wide range of parameters, but many parameters lead to biologically unreasonable shapes of the cell-body, migration speed or directness of movement. However the purpose of these experiments is not to study the effect of the varying parameters on the characteristics of the cell, rather it is to show the variety of behavior of one particular set of parameters.

Videos for selected experimental runs for all of these setups can be found on [20].

The grid $\mathcal{G}$ is chosen to be 500 pixels high and wide ($x_{\max} = 500$ and $y_{\max} = 500$), with non-periodic Dirichlet boundaries. We will be using an twelve-sided cell-body with the parameters: $n = 12$, $k_{\mathrm{mem}} = 0.16$, $l_{\mathrm{mem}} = 16$, $k_{\mathrm{cyto}} = 0.04$, and $l_{\mathrm{cyto}} = 2\,l_{\mathrm{mem}} = 32$. The used neighborhood radius is $d = 2$, and the Gaussian used to compute the stochasticity of movement has $\sigma = 1$. The leading-edge will have $p_{\mathrm{spread}}^{\mathrm{basal}} = p_{\mathrm{detach}}^{\mathrm{basal}} = 0.7$, and $w_{\max} = 60$, and the size of the locality $v = 10$. For all experiments the cell will be initialized at the center of the grid ($x(t = 0) = 250$, and $y(t = 0) = 250$).

The first experiment is designed to verify whether the symmetry-breaking is working as expected. The cell is initialized with the above parameters at $t = 0$ and the simulation is run for 300 time-steps. We repeat this experiment 500 times. We then plot the distribution of angles of displacement over all the 300 time-points (Fig. 4(a)) and the distribution of displacements (Fig. 4(b)).

A second experiment has been designed to show the built-in obstacle avoidance. For this purpose we have filled the grid with obstacles (positions of the grid that are removed from all neighborhoods) and ran 500 simulations for 5000 time-steps (Fig. 5).
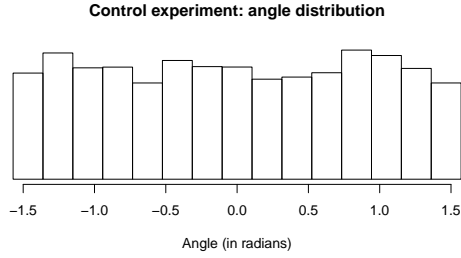
The final experiment is to show how more complex behavior can be implemented. A linear gradient spreads out for 300 pixels from the point at $C_{\mathrm{grad}} = (x = 100, y = 100)$. The values of the gradient decrease linearly from 1, at C_{grad}, to 0 at all positions p, where $\|C_{\mathrm{grad}} - p\| \geq 300$. In this environment we ran two series of 500 cells. One set of standard cells do not climb the gradient, and one set where p_{spread} has been modified to:

$$p_{\mathrm{spread}}^{\mathrm{gradient}}[j, \mathcal{L}(t)] = p_{\mathrm{spread}} + (1 - p_{\mathrm{spread}}^{\mathrm{basal}})G(j),$$
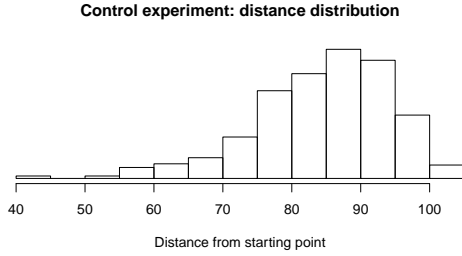
where $G(j)$ is the value of the gradient at position j. Cell migration is simulated for 200 time-steps without any gradient (so as not to mix the effects from the initial symmetry-breaking, and the actual gradient-climbing), and then 3000 time-steps more with the gradient turned on. The trajectories of these two experimental setups have then been plotted (Fig. 6(a)), as well as their displacement from the center of the gradient (Fig. 6(b)).

4. Results

In the first simulation (Fig. 4), we verified that the artificial cell, as implemented in section 2, shows symmetry-breaking, which is an important property

Control experiment: angle distribution

Angle (in radians)

(a)

Control experiment: distance distribution

Distance from starting point

(b)

Figure 4. Symmetry-breaking: 500 experimental runs of a cell moving randomly through the grid, Video 2-3 on [20]. 4(a) Distribution of the angles: the angles of displacements from the centre over the first 300 time-step of 500 independent cell migration simulations. 4(b) Distribution of the distances: the distance from the centre after 300 time-steps of 500 independent cell migration simulations.

Figure 5. Cells in an obstacle course: 500 superposed trajectories of cells on a grid with obstacles. The time flow is from dark to light and the width of the trajectory represents the size of the cell-body, Video 5 on [20].

for the design of further experimental setups. The histogram in Fig. 4(a) confirms rotational invariance of the averaged cell movement from the uniform distribution of all the angles. Additionally, the asymmetry of the histogram in Fig. 4(b) indicates successful symmetry-breaking, as all the cells have moved away from the center of the grid. .

The model as presented here has already built-in obstacle avoidance. As a cell approaches an obstacle, the leading-edge width becomes smaller, which decreases the distance between the centers of mass of the cell-body and leading-edge. As a result, the probability of a novel formation of the leading-edge away from the obstacle is increasing. This is shown in Fig. 5. The overlaid cell-body trajectories from 500 simulations runs never touch any of the obstacles in the environment, as the cell-body "senses" the approaching obstacle through its receding leading-edge.

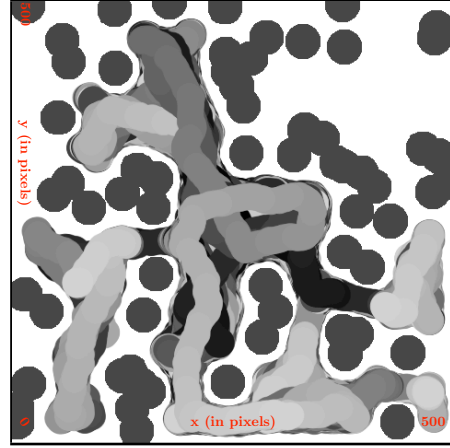As a less direct method of sensing, we investigated how the leading-edge dynamics in the artificial cell

could perform gradient-following. Therefore, we added a term to p_{spread} to increase the probability of spreading for higher values of a gradient, which gives the cell the ability to sense and climb this gradient (Fig. 6). Figure 6(a), shows the heterogeneity of the cell migration behavior. The uniform black background denotes the trajectories of the cells without the additional term. They move randomly within the grid with a higher probability of staying close to the edges. Because of the mechanism of the symmetry-breaking, cells tend to move parallel to the wall. The red trajectories show cells capable of sensing the gradient in the environment. They are consistently attracted and circling around to the highest level of the gradient (Video 4 on [20]). Also note the few simulation runs were the cells to not follow the gradient immediately. In these cases, the cells happen to leave the area of the gradient and continue to move in a random fashion. However, once within its reaches again, they start their tactic behavior. Fig. 6(b) quantifies the strength and consistency of the effect. 99% of measurements are within 70 grid points around the center of the gradient (orange cross in Fig. 6(a)). The sensitivity of the gradient climbing effect is quite remarkable, considering that the maximal difference of $p_{\text{spread}}^{\text{gradient}}$ between opposite ends of the cell-body is one order of magnitude smaller than $p_{\text{spread}}^{\text{basal}}$. Taking 21 grid points as the average width of the cell-body, one obtains $p_{\text{spread}}^{\text{gradient}} = 0.021$ versus $p_{\text{spread}}^{\text{basal}} = 0.7$. The reason for this sensitivity is explained through the small, yet additive forces all acting on the many nodes of the cell-body, which results in a consistent, long-
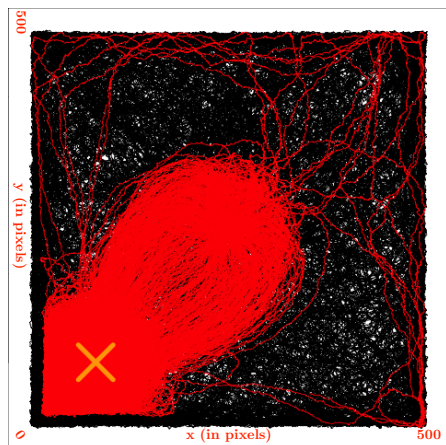
(a)
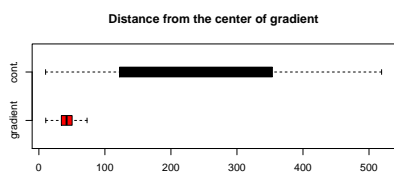
(b)

Figure 6. Gradient-climbing: 500 runs of cells showing gradient-climbing behavior, Video 3-4 on [20]. 6(a) Trajectories: in black, the trajectories of 500 cells for 3000 time steps that do not climb the gradient, Video 3; in red, 500 cells that do, Video 4. The orange cross signifies the centre of the gradient. 6(b) Distances: boxplot of the distances from the center of the gradient after the 3000 time-steps; "cont." and "gradient" denote cells that do not follow or follow gradient-climbing, respectively.

term bias towards the center of the gradient.

5. Conclusion

In this paper we have presented a new approach to the modeling of keratinocyte cell migration. We have developed a phenomenological framework, in which we have decoupled the physical movement from the sensing by defining a connected-spring model of the cell-body and an environment-sensing leading-edge that progresses on a discrete grid, thereby pulling along the cell-body. This model, as we presented in section 2, contains all the properties we set out to implement in the introduction.

Its features have a close resemblance to *in vitro* crawling cells [27]: a rather rigid cell-body that contains most of the organelles that is moved through a highly dynamic and flexible lamellipodial structure. We showed that the model is rotationally symmetric in its function, with either the stochastic cell-body dynamics or the environment breaking this symmetry spontaneously. The cell-body can change its morphology under the influence of the leading-edge. The local integration of the leading-edge at the nodes imitates the way information at the membrane is possibly processed in living cells.

We presented experiments showing the cell model working as expected, in particular, that this implementation includes obstacle-avoidance. We then have presented a modified version of the artificial cell that is very efficiently following gradients.

The model has a very reduced number of parameters (in this implementation seven), all of which are directly relatable to physiological properties of the cell (k_{cyto} and k_{mem} are elasticities, l_{mem} the length of the springs ...). We also managed to design a model that is visually appealing, and understandable by biologists. When working at the interface between computer-sciences and biology it is always important to find a common language to exchange ideas and concepts, having a cell model that is directly understandable helps to generate such a language.

With these properties, we achieve a useable model in which small imbalances in the leading-edge distribution will direct and shape the motion of the artificial cell.

This modeling framework will allow to further investigate into keratinocyte motion, to understand the physicochemical basis of their perception-action loop, i.e. how environmental information and external signals are integrated and processed to form a precise cellular response. The goal is to find, *in silico*, different $p_{\mathrm{spread}}(j, \mathcal{L}_t)$ and $p_{\mathrm{detach}}(j, \mathcal{L}_t)$ functions that link environmental cues to motion, thereby replicating results from *in vivo* experiments, from which testable hypotheses can be deduced.

Lastly we note that our modeling approach is not limited to the simulation of cell migration alone. Its high level of modularity and the distributed nature of the perception-action loop should make it applicable to a wide variety of artificial-life problems. Also the stochastic nature of the leading-edge should allow highly complex non-linear dynamics and emergent behaviors, that could be exploited in a large variety of future theoretical analysis.

References

[1] P. Capdepuy, D. Polani, and C. L. Nehaniv, "Adaptation of the perception-action loop using active channel

sampling," in *Proceedings of the 2008 NASA/ESA Conference on Adaptive Hardware and Systems*, 2008.

[2] G. Gordon, D. M. Kaplan, B. Lankow, D. Y. Little, J. Sherwin, B. A. Suter, and L. Thaler, "Toward an integrated approach to perception and action: conference report and future directions," *Front Syst Neurosci*, vol. 5, p. 20, 2011.

[3] D. A. Fletcher and J. A. Theriot, "An introduction to cell motility for the physical scientist," *Physical Biology*, vol. 1, no. 1, p. T1, 2004.

[4] G. Lowe, M. Meister, and H. C. Berg, "Rapid rotation of flagellar bundles in swimming bacteria," *Nature*, vol. 325, no. 6105, pp. 637–640, Feb. 1987.

[5] S. Ishijima, S. Oshio, and H. Mohri, "Flagellar movement of human spermatozoa," *Gamete Research*, vol. 13, no. 3, pp. 185–197, 1986.

[6] S. J. McRobbie, "Chemotaxis and cell motility in the cellular slime molds," *Crit. Rev. Microbiol.*, vol. 13, no. 4, pp. 335–375, 1986.

[7] C. A. King, "Cell surface interaction of the protozoan Gregarina with concanavalin A beads - implications for models of gregarine gliding," *Cell Biol. Int. Rep.*, vol. 5, no. 3, pp. 297–305, Mar 1981.

[8] D. G. Russell and R. E. Sinden, "The role of the cytoskeleton in the motility of coccidian sporozoites," *J. Cell. Sci.*, vol. 50, pp. 345–359, Aug 1981.

[9] A. Mogilner, T. Elston, H. Wang, and G. Oster, "Molecular motors: Theory," in *Computational Cell Biology*, ser. Interdisciplinary Applied Mathematics, C. Fall, E. Marland, J. Wagner, and J. Tyson, Eds. Springer New York, 2002, vol. 20, pp. 320–353.

[10] ——, "Molecular motors: Examples," in *Computational Cell Biology*, ser. Interdisciplinary Applied Mathematics, C. Fall, E. Marland, J. Wagner, and J. Tyson, Eds. Springer New York, 2002, vol. 20, pp. 354–377.

[11] N. Ogawa, H. Oku, K. Hashimoto, and M. Ishikawa, "A physical model for galvanotaxis of paramecium cell," *Journal of Theoretical Biology*, vol. 242, no. 2, pp. 314 – 328, 2006.

[12] M. Arocena, M. Zhao, J. M. Collinson, and B. Song, "A time-lapse and quantitative modelling analysis of neural stem cell motion in the absence of directional cues and in electric fields," *Journal of Neuroscience Research*, vol. 88, no. 15, pp. 3267–3274, 2010.

[13] A. Mare, A. Jilkine, A. Dawes, V. Grieneisen, and L. Edelstein-Keshet, "Polarization and movement of keratocytes: A multiscale modelling approach," *Bulletin of Mathematical Biology*, vol. 68, pp. 1169–1211, 2006.

[14] C. M. Elliott, B. Stinner, and C. Venkataraman, "Modelling cell motility and chemotaxis with evolving surface finite elements," *Journal of The Royal Society Interface*, vol. 9, no. 76, pp. 3027–3044, Nov. 2012.

[15] J. N. Barker, V. Sarma, R. S. Mitra, V. M. Dixit, and B. J. Nickoloff, "Marked synergism between tumor necrosis factor-alpha and interferon-gamma in regulation of keratinocyte-derived adhesion molecules and chemotactic factors," *J. Clin. Invest.*, vol. 85, no. 2, pp. 605–608, Feb 1990.

[16] R. Grose and S. Werner, "Wound-healing studies in transgenic and knockout mice," *Mol. Biotechnol.*, vol. 28, no. 2, pp. 147–166, Oct 2004.

[17] S. Werner, T. Krieg, and H. Smola, "Keratinocyte-fibroblast interactions in wound healing," *J. Invest. Dermatol.*, vol. 127, no. 5, pp. 998–1008, May 2007.

[18] C. D. McCaig, A. M. Rajnicek, B. Song, and M. Zhao, "Controlling cell behavior electrically: Current views and future potential," *Physiological Reviews*, vol. 85, no. 3, pp. 943–978, 2005.

[19] B. Rubinstein, K. Jacobson, and A. Mogilner, "Multiscale two-dimensional modeling of a motile simple-shaped cell," *Multiscale Model Simul*, vol. 3, no. 2, pp. 413–439, 2005.

[20] www.zbsa.de/projects/frias-hauke-busch/ALife_kera/.

[21] C. Martin, S. F. Pedersen, A. Schwab, and C. Stock, "Intracellular pH gradients in migrating cells," *Am. J. Physiol., Cell Physiol.*, vol. 300, no. 3, pp. C490–495, Mar 2011.

[22] D. Dan, C. Mueller, K. Chen, and J. A. Glazier, "Solving the advection-diffusion equations in biological contexts using the cellular potts model," *Physical Review E (Statistical, Nonlinear, and Soft Matter Physics)*, vol. 72, no. 4, 2005.

[23] V. Braitenberg, *Vehicles: Experiments in Synthetic Psychology*. A Bradford Book, Feb. 1986.

[24] S. Franklin and A. Graesser, "Is it an agent, or just a program?: A taxonomy for autonomous agents," in *Proceedings of the Workshop on Intelligent Agents III, Agent Theories, Architectures, and Languages*, ser. ECAI '96. London, UK, UK: Springer-Verlag, 1997, pp. 21–35.

[25] S. Wolfram, "Statistical mechanics of cellular automata," *Rev. Mod. Phys.*, vol. 55, pp. 601–644, Jul 1983.

[26] S. I. Nishimura, M. Ueda, and M. Sasai, "Non-Brownian dynamics and strategy of amoeboid cell locomotion," *Physical Review E*, vol. 85, no. 4, p. 041909, Apr. 2012. [Online]. Available: http://link.aps.org/doi/10.1103/PhysRevE.85.041909

[27] S. M. Rafelski and J. A. Theriot, "Crawling toward a unified model of cell mobility: spatial and temporal regulation of actin dynamics." *Annual review of biochemistry*, vol. 73, pp. 209–239, 2004.